Cite as: F. Pucci *et al.*, *Science* 10.1126/science.aaf1328 (2016).

SCS macrophages suppress melanoma by restricting tumor-derived vesicle–B cell interactions

Ferdinando Pucci,[1] Christopher Garris,[1,2] Charles P. Lai,[3]* Andita Newton,[1] Christina Pfirschke,[1] Camilla Engblom,[1,2] David Alvarez,[4] Melissa Sprachman,[1] Charles Evavold,[1,2] Angela Magnuson,[1] Ulrich H. von Andrian,[4] Katharina Glatz,[5] Xandra O. Breakefield,[3] Thorsten R. Mempel,[6] Ralph Weissleder,[1] Mikael J. Pittet[1]†

[1]Center for Systems Biology, Massachusetts General Hospital Research Institute, Harvard Medical School, Boston, MA 02114, USA. [2]Graduate Program in Immunology, Harvard Medical School, Boston, MA 02115, USA. [3]Department of Neurology, Massachusetts General Hospital Research Institute, Harvard Medical School, Charlestown, MA 02129, USA. [4]Department of Microbiology and Immunobiology, Harvard Medical School, Boston, MA 02115, USA. [5]Institute of Pathology, University Hospital Basel, 4031 Basel, Switzerland. [6]Center for Immunology and Inflammatory Diseases, Massachusetts General Hospital Research Institute, Harvard Medical School, Charlestown, MA 02129, USA.

*Present address: Institute of Biomedical Engineering, National Tsing Hua University, Hsinchu, Taiwan.

†Corresponding author. E-mail: mpittet@mgh.harvard.edu

Tumor-derived extracellular vesicles (tEVs) are important signals in tumor-host cell communication. Yet, how endogenously produced tEVs impact the host in different areas of the body remains unclear. Here we combine imaging and genetic analysis to track melanoma-derived vesicles at organismal, cellular and molecular scales to show that endogenous tEVs efficiently disseminate via lymphatics and preferentially bind subcapsular sinus (SCS) CD169$^+$ macrophages in tumor-draining lymph nodes (tdLNs) in mice and humans. The CD169$^+$ macrophage layer physically blocks tEV dissemination but is undermined during tumor progression and by therapeutic agents. A disrupted SCS macrophage barrier enables tEVs to enter the LN cortex, interact with B cells and foster tumor-promoting humoral immunity. Thus, CD169$^+$ macrophages may act as tumor suppressors by containing tEV spread and ensuing cancer-enhancing immunity.

Although cancer is driven by tumor cell endogenous genetic mutations, it is also modulated by tumor cell exogenous interactions with host components, including immune cells (*1*). Tumor-induced host immune system activation can occur both within and away from the tumor stroma and may involve different communication signals, including soluble factors (*2*) and tEVs (*3*). tEVs are key candidate conveyors of information between cancer and host immune cells because they can travel long distances in the body without their contents degrading or diluting. tEVs may transfer surface receptors or intracellular material to different host acceptor cells (*4–6*); these processes have all been associated with altered anti-tumor immunity and enhanced cancer progression (*7*). Circulating tEVs also have diagnostic and prognostic potential, as they can be used to detect early cancer stages (*8*) and to predict overall patient survival (*4*) and treatment responses (*9*). Despite increased understanding of tEVs' importance, a critical barrier to progress in the field has been our limited ability to assess the impact of vesicles that are produced in vivo (*7*). To shift current experimental research on tEV-host cell interactions, we combined imaging and genetic approaches to track endogenously produced tEVs and their targets at different resolutions and scales.

We assessed the whole-body biodistribution of tumor-derived material in mice bearing genetically-modified B16F10 melanoma tumors (B16F10–mGLuc), which produce tEVs carrying membrane-bound Gaussia luciferase (mGLuc) (*10*) (fig. S1). Quantification of tEV-bound mGLuc activity in various tissues from B16F10–mGLuc$^+$ tumor-bearing mice not only confirmed that mGLuc$^+$ B16F10–derived tEVs can exit the tumor stroma and relocate to remote organs but also identified the highest relative mGLuc activity in tdLNs when compared to blood, spleen, bone, lung, liver, non-draining LNs (ndLNs) and other tissues (Fig. 1A and fig. S2A). Consistently, we measured higher mGLuc signal in lymph than in plasma (fig. S2B). Control tumors expressing secreted Gaussia luciferase (sGLuc) did not generate bioluminescence activity in tdLNs (fig. S2C).

To decipher endogenous tEVs' interactions in tdLNs at the cellular level, we investigated mice bearing genetically modified B16F10 melanoma tumor cells expressing two membrane-bound reporters, namely the vesicular membrane-associated protein CD63, fused with enhanced green fluorescence protein (CD63-eGFP), and the ubiquitous transmembrane marker dLNGFR (truncated receptor for nerve growth factor) (fig. S3). Flow cytometry-based anal-

yses revealed dLNGFR$^+$ cells in tdLNs but not in ndLNs (Fig. 1B). These tdLNs did not include tumor cells or tumor cell apoptotic bodies (figs. S4 to S6). The dLNGFR signal originated mostly from myeloid cells, not lymphoid cells (Fig. 1C). Among tdLN myeloid cells, the CD11b$^+$ SSC^{LO} fraction, which resembles SCS macrophages (*11*), was dLNGFR$^+$ whereas CD11b$^+$ SSC^{HI} marginal sinus macrophages remained largely dLNGFR$^-$ (Fig. 1D and fig. S7). Multiphoton microscopy and three-dimensional reconstructions of tEV distribution confirmed CD169$^+$ SCS macrophages as a major host cell type interacting with CD63-eGFP$^+$ tEVs in vivo (Fig. 1E and figs. S8 and S9). The vesicles accumulated principally between 10 and 20 μm below the LN capsule and next to CD169$^+$ SCS macrophages, which occupy the space between 20 and 80 μm below the capsule.

We asked whether CD169$^+$ SCS macrophages originate from the tumor stroma where they may initially capture tEVs. B16F10 tumors were implanted in mice ubiquitously expressing the photoconvertible protein Kaede (*12*) and UV light was applied on the tumor site to shift Kaede fluorescence emission from green to red selectively in tumor-infiltrating host cells (fig. S10, A and B). The tdLN SCS macrophages remained green 24h later and therefore did not originate from the tumor stroma (fig. S10C). Photoconverted cells in tdLNs were mostly CD103$^+$ DCs (fig. S10D). These migratory cells might not be involved in carrying tEVs to LNs because analysis of lymph collected from B16F10–mGLuc tumor-bearing mice revealed >10^5 times higher mGLuc activity in cell-free fractions than in cells from lymph (Fig. 1F). These data suggest that tEVs freely disseminate to tdLNs, where they preferentially bind resident SCS macrophages.

To define our findings' relevance for human disease, we examined cancer-free sentinel LN (CF-SLN) biopsies from 13 melanoma patients (table S1). Melanin pigment staining was found selectively in macrophage-like populations in all patients analyzed (figs. S11 and S12, A to C). We then assessed melanoma-derived material by staining CF-SLNs with the mAb clone HMB-45, which is used to pathologically evaluate melanoma metastasis in regional SLNs. HMB-45 reacts with a transmembrane glycoprotein that is part of the gp100 premelanosome complex and is expressed by >80% of melanomas (*13*). Although the SLNs analyzed were melanoma-free (i.e., stage N0), we identified HMB-45$^+$ cells that corresponded to macrophages morphologically and resided mostly near the LN capsule (Fig. 2A and fig. S12D). Serial staining of CF-SLN sections for HMB-45 and the macrophage marker CD68 confirmed that the observed HMB-45$^+$ cells were CD68$^+$ macrophages (Fig. 2B and fig. S13). To interrogate the temporal course of HMB-45$^+$ signal appearance during melanoma progression, we assessed CF-SLNs from patients with distinct clinical stages based on Breslow's thickness (tumor depths ranging from <1 mm to >4 mm). We identified HMB-45$^+$ macrophages in >90% of patients independent of tumor progression (Fig. 2, C and D), suggesting that melanoma-derived material reaches SLNs early in cancer progression, similarly to our observations in mice (fig. S14).

Considering that EVs can deliver intracellular RNAs and proteins into target cells and that such horizontal transfer can shape the fate of acceptor cells (*4*–*6*), we asked whether it characterizes tEV-SCS macrophage interactions. We used transgenic mice that switch on YFP expression upon Cre-mediated recombination and challenged these mice with genetically-modified B16F10 melanoma tumor cells expressing Cre (fig. S15, A to E). Fusion of Cre$^+$ tEVs with host acceptor cells irreversibly induces YFP expression in the target cell. Analysis of B16F10–Cre$^+$ bearing mice identified Cre-induced YFP expression in TAMs; however, tdLN CD169$^+$ SCS macrophages (and all other tdLN cells) remained exclusively YFP$^-$ (Fig. 3, A and B, and fig. S15F). Thus, on their own, endogenous tEVs are unlikely to modulate SCS macrophages through horizontal transfer.

Because SCS macrophage-tEV interactions may regulate tumor progression independently from horizontal transfer, we assessed whether modulating SCS macrophages and/or tEVs affects cancer growth in vivo. We examined *Cd169$^{Dtr/Wt}$* knockin mice in which CD169$^+$ LN macrophages were specifically depleted by diphtheria toxin (DT) injection (figs. S16 and S17). CD169$^+$ LN macrophage removal significantly enhanced B16F10 tumor growth (Fig. 3C). Similarly, specifically depleting CD169$^+$ LN macrophages by subcutaneous administration of clodronate liposomes (figs. S18 and S19) accelerated B16F10 tumor progression in wild-type mice (Fig. 3D). Thus, CD169$^+$ LN macrophages act as "tumor suppressors" in orthotopic B16F10 melanoma; these findings were extended to orthotopic B16F1 melanoma (Fig. 3E) and KP lung adenocarcinoma (Fig. 3F).

To assess whether interactions between endogenous tEVs and SCS macrophages affect tumor progression, we introduced a single copy of either Rab35 wild-type (Rab35^{WT}) or Rab35 dominant-negative mutant (Rab35^{S22N}) (*14*) into B16F10 melanoma cells. These tumors had either normal or impaired capacities to release tEVs (fig. S20). As expected, removing CD169$^+$ macrophages accelerated B16F10 Rab35^{WT} tumor progression; however, Rab35^{S22N} tumors grew similarly with or without CD169$^+$ macrophages (Fig. 3G). The observation that enhanced tumor growth from SCS macrophage ablation only occurs in the context of sufficient tEV production supports a causal link between tEV-SCS macrophage interaction and tumor growth.

We then asked whether cancer disrupts SCS macrophage network organization because pathogens entering LNs can induce such alterations (*15*). Three-dimensional multipho-

ton imaging of tdLNs showed decreased CD169$^+$ SCS macrophage density already on day 6 after tumor challenge (Fig. 3H). This may happen because tdLNs enlarge without expanding their SCS macrophage pool, as indicated by photoconversion (fig. S10), parabiosis (fig. S21A). BrdU (fig. S21B) and Ki67 labeling studies (fig. S21C). These results imply different ontogenesis for TAMs and SCS macrophages because, unlike SCS macrophages, most TAMs derive from circulating monocytes and can divide in some tumors (*16*, *17*). Chemotherapy with paclitaxel and carboplatin (Fig. 3I) and immunotherapy with a small molecule CSF1-R inhibitor (fig. S22) also reduced CD169$^+$ SCS macrophage density. Thus, the SCS macrophage barrier can be disrupted both during the natural course of tumor progression and upon anti-cancer treatments.

Since tEV-SCS macrophage interactions are geographically restricted to tdLNs, yet modulate the outgrowth of distant tumors, they may influence a systemic response to cancer. Indeed, depletion of CD169$^+$ tdLN macrophages on one side only (fig. S23) was sufficient to accelerate both contra- and ipsi-lateral tumor growth (Fig. 4A). We hypothesized that tEVs may bind and regulate discrete host components upon disruption of the SCS macrophage layer. Interestingly, tdLN multiphoton imaging revealed that, without SCS macrophages, tEVs efficiently penetrated the LN cortex (Fig. 4B). These findings indicate that SCS macrophages act as tEV gatekeepers, a capacity that resembles these macrophages' ability to prevent the systemic spread of lymph-borne pathogens (*15*, *18–20*).

Multiphoton imaging of tdLNs in SCS macrophage-depleted mice further revealed that tEVs reached B cell follicles (Fig. 4C). Also, flow cytometry-based analysis of tdLNs identified B cells as the only detectable immune population physically interacting with tEVs in these mice (Fig. 4D and fig. S24A), whereas such interaction was lost if tumors were impaired to secrete tEVs (fig. S24B). B cells remained YFP$^-$ in tdLNs from B16F10–Cre$^+$ tumor-bearing Cre-reporter mice treated with clodronate liposomes, indicating that tEV horizontal gene transfer to B cells does not occur in absence of SCS macrophages (fig. S24A). However, various B cell subsets increased in tdLNs, and concomitantly decreased in ndLNs, as tumors progressed (fig. S24, C and D). The concentration of tumor-infiltrating B cells also increased ~3-fold in SCS macrophage-depleted mice, whereas other immune cells populations remained detectably unchanged (Fig. 4E and fig. S25). To test a causal role for B cells in enhancing melanoma growth after CD169$^+$ LN macrophage ablation, we removed B cells using an anti-CD20 mAb in DT-treated *Cd169$^{Dtr/Wt}$* mice. B cell ablation significantly decreased tumor progression in this experimental setting (Fig. 4F). These data position B cells as tumor-promoting cells, through tEV-B cell interactions that can be suppressed by SCS macrophages.

Because B cells may foster tumor progression by producing auto-antibodies (*21–23*), we tested whether manipulating SCS macrophages modulates IgG responses. Indeed, CD169$^+$ LN macrophage depletion amplified tdLN plasma cells (fig. S26A) and increased both plasma IgG concentration (fig. S26B) and IgG affinity for tumor antigens (fig. S26C). The increased IgG concentration required full-fledged tEV secretion by tumors (fig. S26D). Most importantly, transfer of circulating IgGs from B16F10 tumor-bearing mice, in which SCS macrophages were depleted, significantly accelerated tumor growth in SCS macrophage-competent mice (Fig. 4G and fig. S27). Thus, SCS macrophages can suppress cancer progression at least partly by limiting pro-tumor IgG responses (Fig. 4H).

This study identifies SCS macrophages as tumor-suppressive cells, which contrasts with TAMs that often display tumor-promoting activities (*24*). Yet, tumor progression and at least some therapeutic agents undermine the SCS macrophage barrier, thereby enabling tEV interaction with B cells in the LN cortex and activating tumor-enhancing B cell immunity. Previous studies, which investigated acute responses to pathogens and model foreign antigens, established that SCS macrophages can promote B cell responses (*15*, *20*, *25–27*). The present data suggest that SCS macrophages can also provide a physical barrier to B cell activity under specific circumstances. It is possible that SCS macrophages acquire different functions when exposed continuously to inflammatory triggers or in the context of sterile inflammation. Additionally, tEVs may have unique properties that prevent their presentation by SCS macrophages to B cells or that alter SCS macrophage functions in vivo. Thus far, macrophage-targeting therapies to treat cancer are mostly aimed at depleting these cells indiscriminately (*28*). Instead our results favor therapeutic approaches that limit harmful TAM functions while leaving SCS macrophages unaffected. Whether it is possible to selectively expand SCS macrophages to control cancer also deserves consideration. In support of this scenario, a high density of CD169$^+$ macrophages in regional LNs positively correlated with longer overall survival in patients with colorectal carcinoma (*29*).

REFERENCES AND NOTES

1. D. Hanahan, R. A. Weinberg, Hallmarks of cancer: The next generation. *Cell* **144**, 646–674 (2011). Medline doi:10.1016/j.cell.2011.02.013
2. S. S. McAllister, R. A. Weinberg, The tumour-induced systemic environment as a critical regulator of cancer progression and metastasis. *Nat. Cell Biol.* **16**, 717–727 (2014). Medline doi:10.1038/ncb3015
3. M. Colombo, G. Raposo, C. Théry, Biogenesis, secretion, and intercellular interactions of exosomes and other extracellular vesicles. *Annu. Rev. Cell Dev. Biol.* **30**, 255–289 (2014). Medline doi:10.1146/annurev-cellbio-101512-122326
4. H. Peinado, M. Alečković, S. Lavotshkin, I. Matei, B. Costa-Silva, G. Moreno-Bueno, M. Hergueta-Redondo, C. Williams, G. García-Santos, C. Ghajar, A. Nitadori-Hoshino, C. Hoffman, K. Badal, B. A. Garcia, M. K. Callahan, J. Yuan, V. R. Martins, J. Skog, R. N. Kaplan, M. S. Brady, J. D. Wolchok, P. B. Chapman, Y.

Kang, J. Bromberg, D. Lyden, Melanoma exosomes educate bone marrow progenitor cells toward a pro-metastatic phenotype through MET. *Nat. Med.* **18**, 883–891 (2012). Medline doi:10.1038/nm.2753
5. J. Skog, T. Würdinger, S. van Rijn, D. H. Meijer, L. Gainche, M. Sena-Esteves, W. T. Curry Jr., B. S. Carter, A. M. Krichevsky, X. O. Breakefield, Glioblastoma microvesicles transport RNA and proteins that promote tumour growth and provide diagnostic biomarkers. *Nat. Cell Biol.* **10**, 1470–1476 (2008). Medline doi:10.1038/ncb1800
6. A. Zomer, C. Maynard, F. J. Verweij, A. Kamermans, R. Schäfer, E. Beerling, R. M. Schiffelers, E. de Wit, J. Berenguer, S. I. Ellenbroek, T. Wurdinger, D. M. Pegtel, J. van Rheenen, In vivo imaging reveals extracellular vesicle-mediated phenocopying of metastatic behavior. *Cell* **161**, 1046–1057 (2015). Medline doi:10.1016/j.cell.2015.04.042
7. F. Pucci, M. J. Pittet, Molecular pathways: Tumor-derived microvesicles and their interactions with immune cells in vivo. *Clin. Cancer Res.* **19**, 2598–2604 (2013). Medline
8. S. A. Melo, L. B. Luecke, C. Kahlert, A. F. Fernandez, S. T. Gammon, J. Kaye, V. S. LeBleu, E. A. Mittendorf, J. Weitz, N. Rahbari, C. Reissfelder, C. Pilarsky, M. F. Fraga, D. Piwnica-Worms, R. Kalluri, Glypican-1 identifies cancer exosomes and detects early pancreatic cancer. *Nature* **523**, 177–182 (2015). Medline
9. H. Shao, J. Chung, K. Lee, L. Balaj, C. Min, B. S. Carter, F. H. Hochberg, X. O. Breakefield, H. Lee, R. Weissleder, Chip-based analysis of exosomal mRNA mediating drug resistance in glioblastoma. *Nat. Commun.* **6**, 6999 (2015). Medline doi:10.1038/ncomms7999
10. C. P. Lai, O. Mardini, M. Ericsson, S. Prabhakar, C. A. Maguire, J. W. Chen, B. A. Tannous, X. O. Breakefield, Dynamic biodistribution of extracellular vesicles in vivo using a multimodal imaging reporter. *ACS Nano* **8**, 483–494 (2014). Medline
11. E. E. Gray, J. G. Cyster, Lymph node macrophages. *J. Innate Immun.* **4**, 424–436 (2012). Medline doi:10.1159/000337007
12. A. M. Magnuson, G. M. Thurber, R. H. Kohler, R. Weissleder, D. Mathis, C. Benoist, Population dynamics of islet-infiltrating cells in autoimmune diabetes. *Proc. Natl. Acad. Sci. U.S.A.* **112**, 1511–1516 (2015). Medline doi:10.1073/pnas.1423769112
13. H. Yaziji, A. M. Gown, Immunohistochemical markers of melanocytic tumors. *Int. J. Surg. Pathol.* **11**, 11–15 (2003). Medline doi:10.1177/106689690301100103
14. H. Stenmark, Rab GTPases as coordinators of vesicle traffic. *Nat. Rev. Mol. Cell Biol.* **10**, 513–525 (2009). doi:10.1038/nrm2728
15. M. Gaya, A. Castello, B. Montaner, N. Rogers, C. Reis e Sousa, A. Bruckbauer, F. D. Batista, Inflammation-induced disruption of SCS macrophages impairs B cell responses to secondary infection. *Science* **347**, 667–672 (2015). Medline doi:10.1126/science.aaa1300
16. V. Cortez-Retamozo, M. Etzrodt, A. Newton, P. J. Rauch, A. Chudnovskiy, C. Berger, R. J. Ryan, Y. Iwamoto, B. Marinelli, R. Gorbatov, R. Forghani, T. I. Novobrantseva, V. Koteliansky, J. L. Figueiredo, J. W. Chen, D. G. Anderson, M. Nahrendorf, F. K. Swirski, R. Weissleder, M. J. Pittet, Origins of tumor-associated macrophages and neutrophils. *Proc. Natl. Acad. Sci. U.S.A.* **109**, 2491–2496 (2012). Medline doi:10.1073/pnas.1113744109
17. R. A. Franklin, W. Liao, A. Sarkar, M. V. Kim, M. R. Bivona, K. Liu, E. G. Pamer, M. O. Li, The cellular and molecular origin of tumor-associated macrophages. *Science* **344**, 921–925 (2014). Medline doi:10.1126/science.1252510
18. M. Iannacone, E. A. Moseman, E. Tonti, L. Bosurgi, T. Junt, S. E. Henrickson, S. P. Whelan, L. G. Guidotti, U. H. von Andrian, Subcapsular sinus macrophages prevent CNS invasion on peripheral infection with a neurotropic virus. *Nature* **465**, 1079–1083 (2010). doi:10.1038/nature09118
19. W. Kastenmüller, P. Torabi-Parizi, N. Subramanian, T. Lämmermann, R. N. Germain, A spatially-organized multicellular innate immune response in lymph nodes limits systemic pathogen spread. *Cell* **150**, 1235–1248 (2012). Medline doi:10.1016/j.cell.2012.07.021
20. E. A. Moseman, M. Iannacone, L. Bosurgi, E. Tonti, N. Chevrier, A. Tumanov, Y. X. Fu, N. Hacohen, U. H. von Andrian, B cell maintenance of subcapsular sinus macrophages protects against a fatal viral infection independent of adaptive immunity. *Immunity* **36**, 415–426 (2012). Medline doi:10.1016/j.immuni.2012.01.013
21. P. Andreu, M. Johansson, N. I. Affara, F. Pucci, T. Tan, S. Junankar, L. Korets, J. Lam, D. Tawfik, D. G. DeNardo, L. Naldini, K. E. de Visser, M. De Palma, L. M. Coussens, FcRγ activation regulates inflammation-associated squamous carcinogenesis. *Cancer Cell* **17**, 121–134 (2010). Medline doi:10.1016/j.ccr.2009.12.019
22. K. E. de Visser, L. V. Korets, L. M. Coussens, De novo carcinogenesis promoted by chronic inflammation is B lymphocyte dependent. *Cancer Cell* **7**, 411–423 (2005). Medline doi:10.1016/j.ccr.2005.04.014
23. P. M. Hogarth, G. A. Pietersz, Fc receptor-targeted therapies for the treatment of inflammation, cancer and beyond. *Nat. Rev. Drug Discov.* **11**, 311–331 (2012). Medline doi:10.1038/nrd2909
24. T. A. Wynn, A. Chawla, J. W. Pollard, Macrophage biology in development, homeostasis and disease. *Nature* **496**, 445–455 (2013). Medline doi:10.1038/nature12034
25. Y. R. Carrasco, F. D. Batista, B cells acquire particulate antigen in a macrophage-rich area at the boundary between the follicle and the subcapsular sinus of the lymph node. *Immunity* **27**, 160–171 (2007). Medline doi:10.1016/j.immuni.2007.06.007
26. T. Junt, E. A. Moseman, M. Iannacone, S. Massberg, P. A. Lang, M. Boes, K. Fink, S. E. Henrickson, D. M. Shayakhmetov, N. C. Di Paolo, N. van Rooijen, T. R. Mempel, S. P. Whelan, U. H. von Andrian, Subcapsular sinus macrophages in lymph nodes clear lymph-borne viruses and present them to antiviral B cells. *Nature* **450**, 110–114 (2007). Medline doi:10.1038/nature06287
27. T. G. Phan, J. A. Green, E. E. Gray, Y. Xu, J. G. Cyster, Immune complex relay by subcapsular sinus macrophages and noncognate B cells drives antibody affinity maturation. *Nat. Immunol.* **10**, 786–793 (2009). Medline doi:10.1038/ni.1745
28. C. H. Ries, S. Hoves, M. A. Cannarile, D. Rüttinger, CSF-1/CSF-1R targeting agents in clinical development for cancer therapy. *Curr. Opin. Pharmacol.* **23**, 45–51 (2015). Medline doi:10.1016/j.coph.2015.05.008
29. K. Ohnishi, Y. Komohara, Y. Saito, Y. Miyamoto, M. Watanabe, H. Baba, M. Takeya, CD169-positive macrophages in regional lymph nodes are associated with a favorable prognosis in patients with colorectal carcinoma. *Cancer Sci.* **104**, 1237–1244 (2013). Medline doi:10.1111/cas.12212
30. M. Amendola, M. A. Venneri, A. Biffi, E. Vigna, L. Naldini, Coordinate dual-gene transgenesis by lentiviral vectors carrying synthetic bidirectional promoters. *Nat. Biotechnol.* **23**, 108–116 (2005). Medline doi:10.1038/nbt1049
31. M. De Palma, L. Naldini, Transduction of a gene expression cassette using advanced generation lentiviral vectors. *Methods Enzymol.* **346**, 514–529 (2002). Medline doi:10.1016/S0076-6879(02)46074-0
32. M. DuPage, A. L. Dooley, T. Jacks, Conditional mouse lung cancer models using adenoviral or lentiviral delivery of Cre recombinase. *Nat. Protoc.* **4**, 1064–1072 (2009). Medline doi:10.1038/nprot.2009.95
33. S. Massberg, P. Schaerli, I. Knezevic-Maramica, M. Köllnberger, N. Tubo, E. A. Moseman, I. V. Huff, T. Junt, A. J. Wagers, I. B. Mazo, U. H. von Andrian, Immunosurveillance by hematopoietic progenitor cells trafficking through blood, lymph, and peripheral tissues. *Cell* **131**, 994–1008 (2007). Medline doi:10.1016/j.cell.2007.09.047
34. S. M. Pyonteck, L. Akkari, A. J. Schuhmacher, R. L. Bowman, L. Sevenich, D. F. Quail, O. C. Olson, M. L. Quick, J. T. Huse, V. Teijeiro, M. Setty, C. S. Leslie, Y. Oei, A. Pedraza, J. Zhang, C. W. Brennan, J. C. Sutton, E. C. Holland, D. Daniel, J. A. Joyce, CSF-1R inhibition alters macrophage polarization and blocks glioma progression. *Nat. Med.* **19**, 1264–1272 (2013). Medline doi:10.1038/nm.3337
35. F. Pucci, M. A. Venneri, D. Biziato, A. Nonis, D. Moi, A. Sica, C. Di Serio, L. Naldini, M. De Palma, A distinguishing gene signature shared by tumor-infiltrating Tie2-expressing monocytes, blood "resident" monocytes, and embryonic macrophages suggests common functions and developmental relationships. *Blood* **114**, 901–914 (2009). Medline doi:10.1182/blood-2009-01-200931
36. E. E. Gray, S. Friend, K. Suzuki, T. G. Phan, J. G. Cyster, Subcapsular sinus macrophage fragmentation and CD169$^+$ bleb acquisition by closely associated IL-17-committed innate-like lymphocytes. *PLOS ONE* **7**, e38258 (2012). Medline doi:10.1371/journal.pone.0038258
37. A. S. Payne, L. A. Cornelius, The role of chemokines in melanoma tumor growth and metastasis. *J. Invest. Dermatol.* **118**, 915–922 (2002). Medline doi:10.1046/j.1523-1747.2002.01725.x
38. K. Asano, A. Nabeyama, Y. Miyake, C. H. Qiu, A. Kurita, M. Tomura, O. Kanagawa, S. Fujii, M. Tanaka, CD169-positive macrophages dominate antitumor immunity by crosspresenting dead cell-associated antigens. *Immunity* **34**, 85–95 (2011). Medline doi:10.1016/j.immuni.2010.12.011

ACKNOWLEDGMENTS

The authors thank M. Ericsson for helping with electron microscopy studies, T. Murooka for multiphoton microscopy experiments and S. Mordecai for imaging flow cytometry. The data presented in this manuscript are tabulated in the main paper and in the supplementary materials. This work was supported in part by the Samana Cay MGH Research Scholar Fund and NIH grants R21-CA190344, P50-CA86355 and R01-AI084880 (to M.J.P.), U54-CA126515, T32CA79443, RO1EB010011, 1R01CA164448, 1R33CA202064 (to R.W.), P01-CA069246 (to X.O.B. and R.W.), U19 CA179563 (to X.O.B. and T.R.M.), R01 AI097052 (to T.R.M.) and F31-CA196035 (to C.G.); EMBO long-term fellowship and MGH ECOR Funds for Medical Discovery Fellowship (to F.P.); Deutsche Forschungsgemeinschaft PF809/1-1 (to C.P.); Canadian Institutes of Health Research Postdoctoral Fellowship (to C.P.L.); and Boehringer Ingelheim Funds (to C.E.).

SUPPLEMENTARY MATERIALS

www.sciencemag.org/cgi/content/full/science.aaf1328/DC1
Materials and Methods
Figs. S1 to S27
Table S1
References (*30*–*38*)

21 December 2015; accepted 25 February 2016
Published online 17 March 2016
10.1126/science.aaf1328

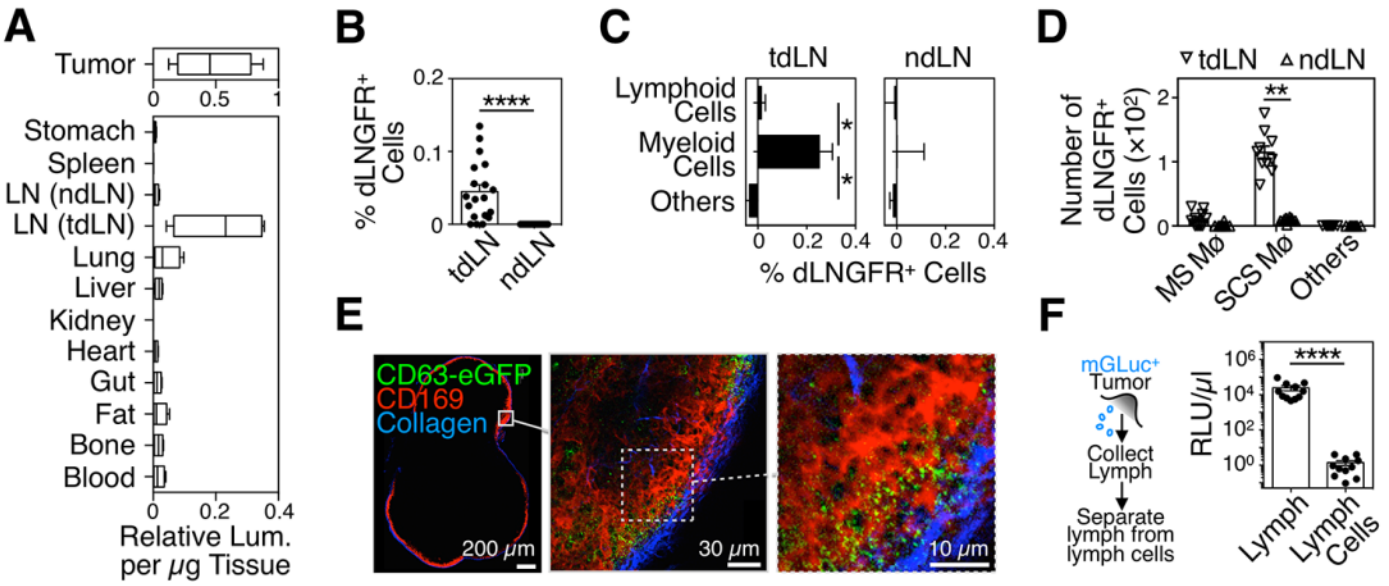

Fig. 1. Endogenous tEVs disseminate via lymph and interact with tumor-draining LN SCS macrophages. (**A**) Relative mGLuc luminescence activity (per µg tissue) in various organs isolated from mice carrying mGLuc$^+$ B16F10 melanoma tumors on week 2 after tumor challenge (2 independent experiments, n = 8-10). (**B** to **E**) Quantification of host dLNGFR$^+$ cells in (B) total tdLN and ndLN cells, (C) lymphoid/myeloid cell fractions, and (D) macrophage subsets isolated from mice carrying dLNGFR$^+$ B16F10 melanoma tumors on week 2 after tumor challenge (2 independent experiments, n > 10). (E) Representative multiphoton micrographs of an explanted tdLN from a mouse carrying CD63-eGFP$^+$ B16F10 melanoma on week 2 after tumor challenge (2 independent experiments; n = 6). (**F**) Experimental outline of lymph collection (left) and quantification of mGLuc signal in cell-free lymph and cells from lymph (2 independent experiments; n = 11). $^{**}P < 0.01$; $^{****}P < 0.0001$; Mann Whitney test. Mø = macrophage; MS = medullary sinus; ndLN = non-draining LN; SCS = subcapsular sinus; TAM = tumor-associated macrophages; tdLN = tumor-draining LN; tEV = tumor-derived extracellular vesicles.

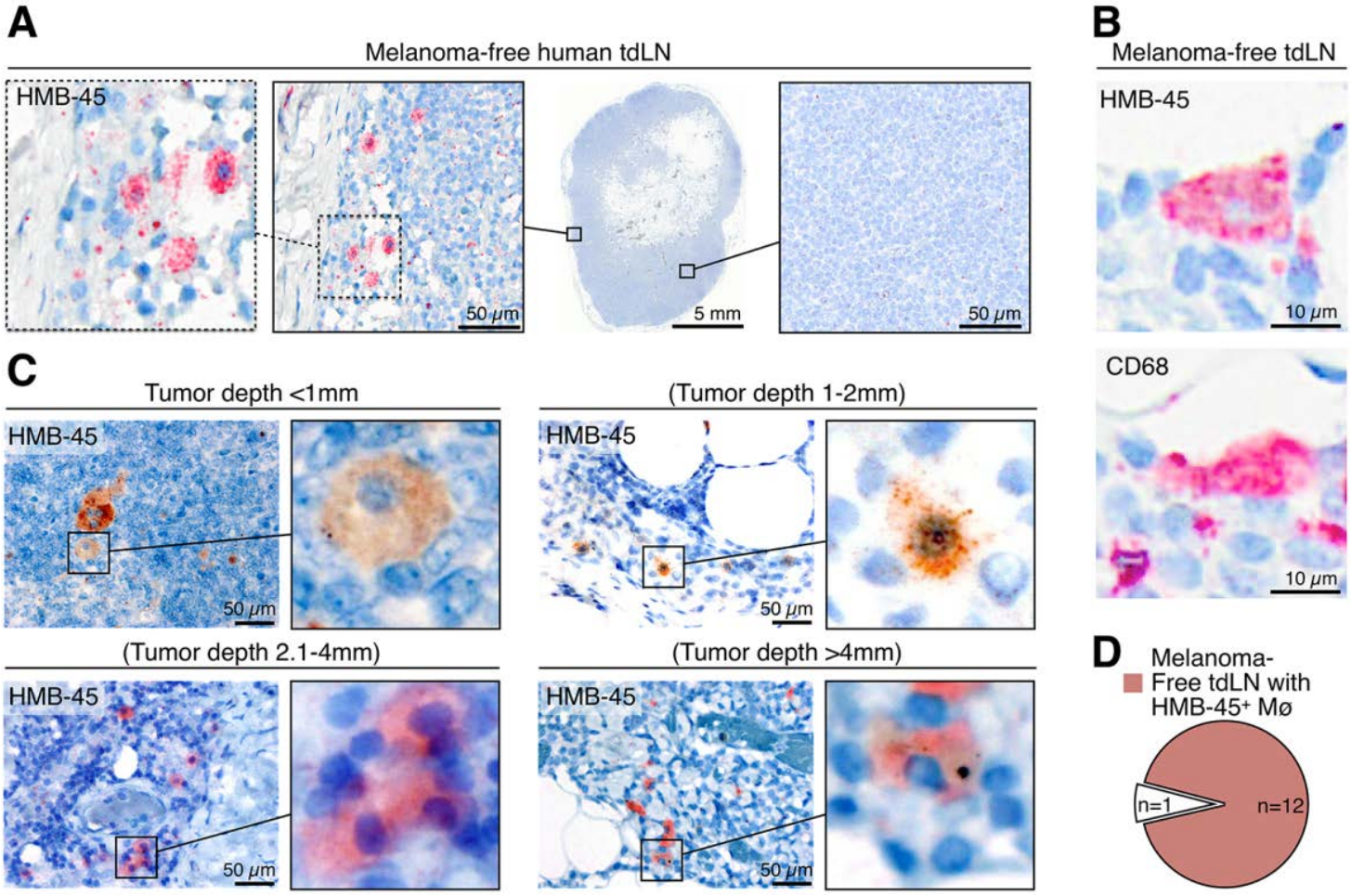

Fig. 2. Human SCS macrophages collect tumor-derived materials in melanoma-free tumor-draining LNs. (**A**) Immunohistochemistry for the melanoma marker HMB-45 (red) in a tdLN from a melanoma-free (i.e., stage N0) patient. The tissue was counterstained with hematoxylin (blue). (**B**) Immunohistochemistry for HMB-45 melanoma (top) and CD68 macrophage markers (bottom) in sequential sections from a melanoma-free (i.e., stage N0) tdLN. (**C**) HMB-45 immunohistochemistry (brown or red) in tdLNs from melanoma-free patients with different tumor stages (according to American Joint Committee on Cancer guidelines). Primary tumor depth is indicated above each image. Tissues were counterstained with hematoxylin (blue). (**D**) Pie chart illustrating the fraction of patients containing HMB-45$^+$ macrophages in melanoma-free tdLNs. tdLN = tumor-draining LN; Mø = macrophage.

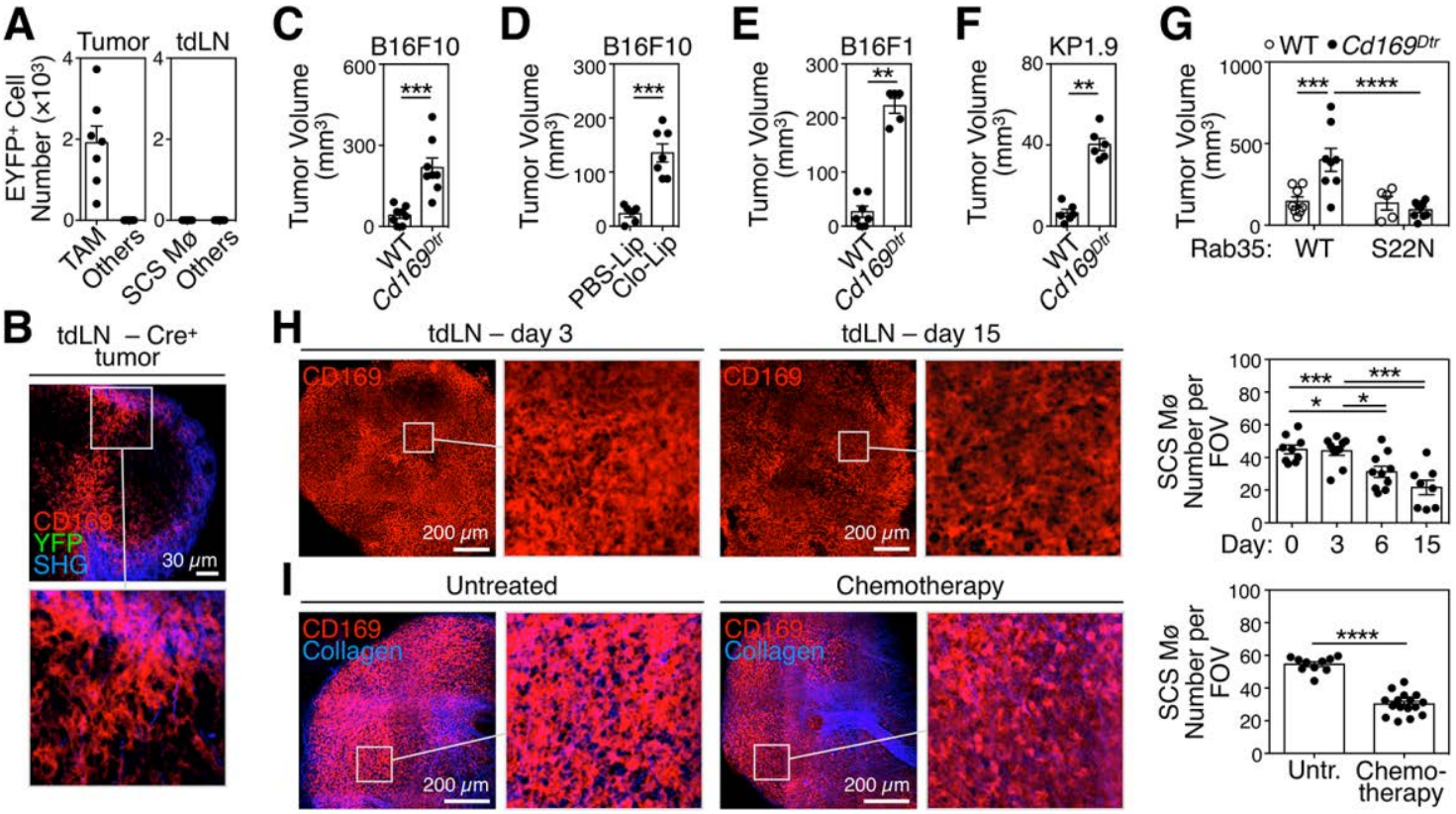

Fig. 3. tEV-SCS macrophage interactions suppress tumor growth. (**A**) Number of eYFP⁺ TAMs, SCS Mø and other cells on week 2 after challenging Cre-reporter mice with Cre⁺ B16F10 tumors (2 independent experiments, n = 8). (**B**) Multiphoton micrographs of LNs draining Cre⁺ tumors (1 experiment, n = 3). (**C**) B16F10 tumor volume in wild-type or *Cd169*$^{Dtr/Wt}$ mice, all treated with DT i.p. (2 independent experiments, n = 8). (**D**) B16F10 tumor volume in wild-type mice treated with PBS-Lip or Clo-Lip s.c. (2 independent experiments; n = 6-7). (**E**) B16F1 melanoma tumor volume in wild-type or *Cd169*$^{Dtr/Wt}$ mice, all treated with DT i.p. (n = 5-7) (**F**) KP1.9 lung adenocarcinoma tumor volume in wild-type or *Cd169*$^{Dtr/Wt}$ mice, all treated with DT i.p. (n = 6) (**G**) B16F10 tumor volume in wild-type or *Cd169*$^{Dtr/Wt}$ mice, all treated with DT i.p., and challenged with tumors expressing either WT or S22N mutant Rab35 (n = 5-8). (**H**) Left: multiphoton micrographs (2D projections of 30 high resolution optical sections spanning the whole LN with 2 μm Z-spacing) of tdLNs on d 3, 6 and 15 after B16F10 tumor challenge (n = 2-3). Right: quantification of SCS Mø barrier disruption measured as CD169⁺ SCS macrophage number per field of view. (**I**) Left: multiphoton micrographs [obtained similarly as in (H)] of inguinal LNs one week after starting i.p. Paclitaxel/Carboplatin injections, 3 times per week (n = 4). Right: quantification as in (H). *P < 0.05; **P < 0.01; ***P < 0.001; ****P < 0.0001; Mann Whitney test for (C), (D), (E), (F), and (I), Two-way ANOVA for (G), One-way ANOVA with Tukey's multiple comparisons test for (H). Clo-Lip = clodronate-loaded liposomes; DT = diphtheria toxin; FOV = field of view; ndLN = non tumor-draining LN; PBS-Lip = PBS-loaded liposomes; SCS Mø = sub-capsular sinus macrophages; TAM = tumor-associated macrophages; tdLN = tumor-draining LN; tEV = tumor-derived extracellular vesicles; Untr. = Untreated.

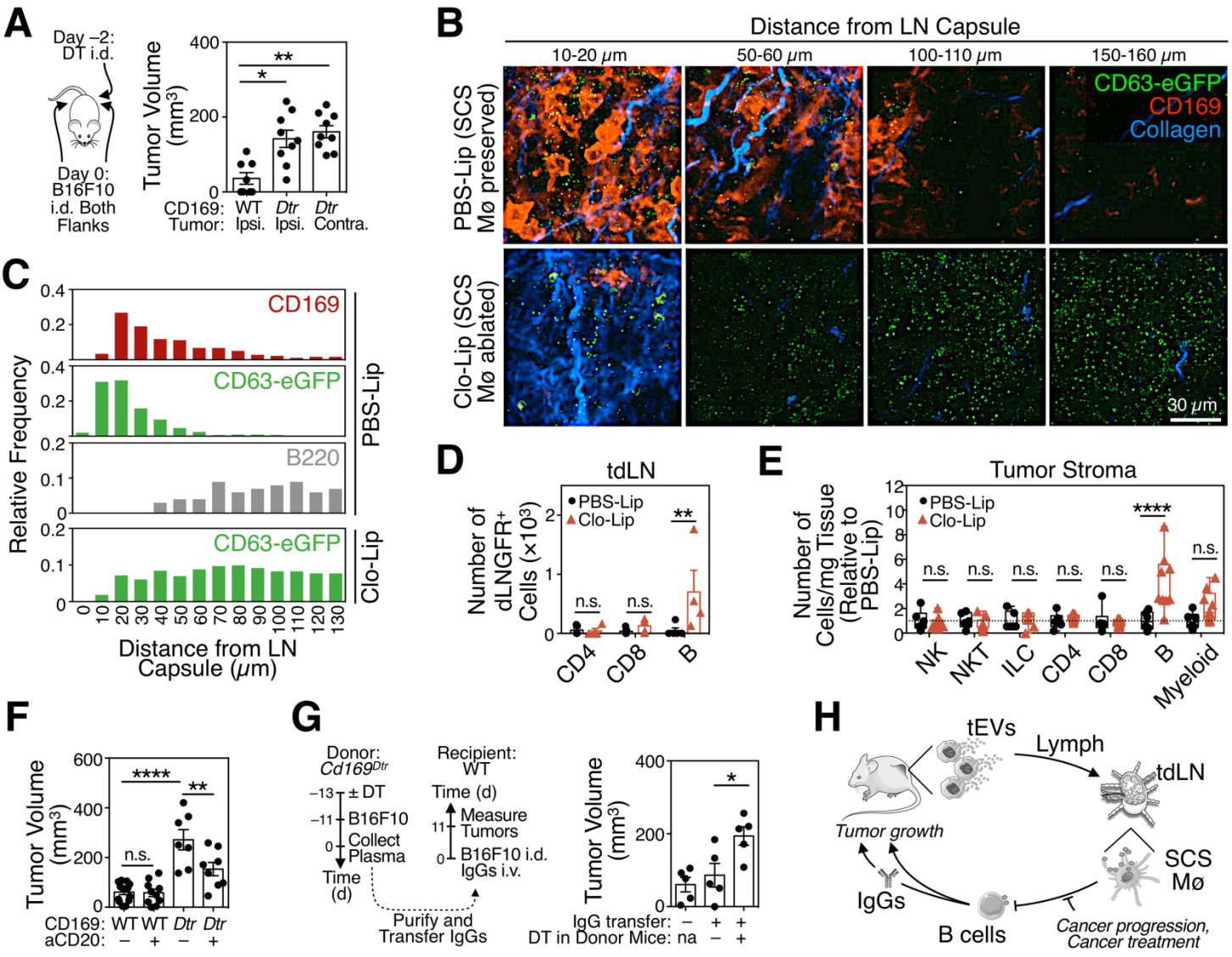

Fig. 4. tEV-SCS macrophage interactions suppress tumor-promoting B cell immunity. (**A**) Tumor volumes in *Cd169*$^{Dtr/Wt}$ mice locally treated with DT s.c. on one side and challenged with B16F10 tumors on both flanks i.d. (n = 9). (**B**) Multiphoton micrographs of tdLNs from CD63-eGFP^{+} B16F10 bearing mice (treated with PBS-Lip or Clo-Lip s.c.) and imaged at the indicated depth below the LN capsule (blue). CD169 in red and eGFP in green. (2 independent experiments; n = 3) (**C**) Distance between the indicated entities (CD169^{+} cells, CD63-eGFP^{+} tEVs and B220^{+} cells) and the LN capsule, plotted as relative frequency versus position. (**D**) Flow cytometry-based quantification of dLNGFR^{+} lymphocyte subsets in tdLNs from dLNGFR^{+} B16F10 melanoma-bearing mice treated with PBS-Lip or Clo-Lip s.c. (n = 4-5). (**E**) Flow cytometry based quantification of different cell types in B16F10 tumors from mice treated with PBS-Lip or Clo-Lip (data are normalized to PBS-Lip-treated mice; 2 independent experiments; n = 9). (**F**) B16F10 tumor volumes (d 9) in WT and *Cd169*$^{Dtr/Wt}$ mice treated with DT i.p. and/or with anti-CD20 depleting mAb. (n = 7-10) (**G**) B16F10 tumor volumes in WT recipient mice that received IgGs (25 μg) isolated from plasma of *Cd169*$^{Dtr/Wt}$ donor mice treated with PBS or DT i.p. (n = 5). Mice that did not receive IgGs were used as controls. (**H**) Proposed model. *P<0.05; **P<0.01; ***P<0.001; n.s. = not significant. Kruskal-Wallis test with Dunn's multiple comparisons test for (A), Two-way ANOVA with Sidak's multiple comparisons test for (D) and (E), One-way ANOVA with Tukey's multiple comparisons test for (F) and (G). aCD20 = anti-CD20 mAb; Clo-Lip = clodronate-loaded liposomes; Contra = contralateral; DT = diphtheria toxin; DTR = DT receptor; ILC = innate lymphoid cells; Ipsi = Ipsilateral; Mø = macrophages; NK = natural killer cells; NKT = natural killer T cells; PBS-Lip = PBS-loaded liposomes; tdLN = tumor-draining LN; tEV = tumor-derived extracellular vesicles.